Josephson and noise scanning tunneling microscopy on conventional, unconventional and disordered superconductors

Chatzopoulos, D.

4

Impurity states in Fe(Te,Se)

By using scanning tunneling microscopy (STM) we find and characterize dispersive, energy-symmetric in-gap states in the iron-based superconductor $FeTe_{0.55}Se_{0.45}$*, a material that exhibits signatures of topological superconductivity, and Majorana bound states at vortex cores or at impurity locations. We use a superconducting STM tip for enhanced energy resolution, which enables us to show that impurity states can be tuned through the Fermi level with varying tip-sample distance. We find that the impurity state is of the Yu-Shiba-Rusinov (YSR) type, and argue that the energy shift is caused by the low superfluid density in* $FeTe_{0.55}Se_{0.45}$*, which allows the electric field of the tip to slightly penetrate the sample. We model the newly introduced tip-gating scenario within the single-impurity Anderson model and find good agreement to the experimental data.*

This chapter and the corresponding Appendix B have been published as Nature Communications **12**, 298 (2021).

4.1. Introduction

The putative $s_{\pm}$ superconductor $FeTe_{0.55}Se_{0.45}$ is peculiar because it has a low Fermi energy and an unusually low and inhomogeneous superfluid density [1–7]. It has been predicted to host a topological superfluid and Majorana zero-mode states [8–10]. These predictions have been supported by recent experiments: photoemission has discovered Dirac-like dispersion of a surface state [11] while tunneling experiments have concentrated on in-gap states in vortex cores, which have been interpreted as Majorana bound states [12, 13] since the low Fermi energy allows to distinguish them from conventional low-energy Caroli-Matricon-de Gennes states [14].

In-gap states have a long history of shining light into the properties of different host materials, and have allowed to bring insight into gap symmetry and structure, symmetry breaking, or the absence of scattering in topological defects, to name a few [15–24]. Impurity bound states have also been investigated in chains or arrays of magnetic impurities on superconducting surfaces where they can lead to Majorana edge-states [25–28]. In the case of $FeTe_{0.55}Se_{0.45}$, zero-bias in-gap resonances have become a primary way to identify Majorana bound states at magnetic impurity sites or in vortex cores. At impurity sites, robust zero-bias peaks have been reported at interstitial iron locations which suggest the presence of Majorana physics [29]. In addition, very recently STM experiments reported signatures of reversibility between magnetic impurity bound states and Majorana zero modes by varying the tip-sample distance on magnetic adatoms [30]. Interestingly, there have also been signatures of spatially varying in-gap impurity states [31, 32] which are not yet understood.

Here we report the detection of in-gap states at sub-surface impurities, which are spatially dispersing, i.e. they change energy when moving away from the impurity site by a distance of Δy. The energy can also be tuned by changing the tip-sample distance (Δd). We argue that the most likely explanation of our observations involves a magnetic impurity state of the YSR type affected by the electric field of the tip. We show good agreement between our experimental findings and the single impurity Anderson model.

4.2. Methods

We use $FeTe_{0.55}Se_{0.45}$ samples with a critical temperature of $T_C = 14.5$ K. They are cleaved at ~ 30 K in ultra-high vacuum, and immediately inserted into a modified Unisoku STM at a base temperature of 2.2 K, for preventing surface reconstruction and contamination. Standard lock-in technique is employed for all the tunnelling conductance measurements at 887 Hz. To increase the energy resolution, we perform all tunneling experiments using a superconducting tip, made by indenting mechanically grinded Pt-Ir tips into a clean Pb(111) surface. The latter was first cleaned by repetitive cycles of Ar sputtering ($P_{base} \sim 5 \times 10^{-5}$ mbar) followed by thermal annealing.

With the superconducting tip and to leading order in the tunnel coupling, the current-voltage ($I - V$) characteristic curves are proportional to the convolution of

the density of states of Bogoliubov quasiparticles in the tip and the sample

$$I(\mathbf{r},V) \sim \int D_{\mathrm{t}}(\omega+eV)D_{\mathrm{s}}(\mathbf{r},\omega)[f(\omega,T)-f(\omega+eV,T)]d\omega, \tag{4.1}$$

where $D_{\mathrm{s(t)}}$ is the density of states of the quasiparticles in the sample (tip), $f(\omega,T)$ is the Fermi-Dirac distribution at temperature T and e is the electron charge. In such a superconducting tunnel junction the coherence peaks in the conductance spectra, $dI/dV(\mathbf{r},V)$, appear at energies: $\pm(\Delta_{\mathrm{t}}+\Delta_{\mathrm{s}})$, where $\Delta_{\mathrm{s(t)}}$ is the quasiparticle excitation gap of the sample (tip). In addition, the energy resolution is far better than the conventional thermal broadening of $\sim 3.5k_{\mathrm{B}}T$ (k_{B} is the Boltzmann constant) since it is enhanced by the sharpness of the coherence peaks of D_{t} [33–35].

To obtain the intrinsic local density of states (LDOS) of the sample, $D_{\mathrm{s}}(\mathbf{r},\omega)$, we numerically deconvolute our measured $dI/dV(\mathbf{r},V)$ spectra while retaining the enhanced energy resolution. For this, we use our knowledge of the density of states of the tip with a gap of $\Delta_{\mathrm{t}} = 1.3$ meV from test experiments on the Pb(111) surface using the same tip.

Deconvolution of spectral density

In order to obtain the local density of states (LDOS) of the sample we use a deconvolution algorithm which subtracts the density of states of the tip from the measured spectra. We follow the same procedure as in Refs. [36, 37]. The first step is to characterize the tip density of states. This is done by taking spectra with a Pb tip on Pb as described elsewhere [3]. We fit these spectra with

$$\left(\frac{dI}{dV}\right) = \frac{1}{eR_{\mathrm{N}}}\int\left\{\frac{\partial D_{\mathrm{t}}(\omega+eV)}{\partial V}[f(\omega)-f(\omega+eV)] - D_{\mathrm{t}}(\omega+eV)\frac{\partial f(\omega+eV)}{\partial V}\right\}D_{\mathrm{t}}(\omega)d\omega, \tag{4.2}$$

in order to extract the gap Δ_{t} and the broadening term γ_{t} of the tip. For the $D_{\mathrm{t}}(\omega,\Delta_{\mathrm{t}},\gamma_{\mathrm{t}})$, a modified Dynes formula is used

$$D_{\mathrm{t}}(\omega,\Delta_{\mathrm{t}},\gamma_{\mathrm{t}}) = \mathrm{Re}\left[\mathrm{sgn}(\omega)\frac{\omega}{\sqrt{\omega^2+2i\gamma_{\mathrm{t}}\omega-\Delta_{\mathrm{t}}^2}}\right]. \tag{4.3}$$

Good agreement is found for $\Delta_{\mathrm{t}} = 1.3$ meV and $\gamma_{\mathrm{t}} = 45$ μeV. Next, we discretize the theoretical tunneling formula for the differential conductance

$$\left(\frac{dI}{dV}\right)_j = \frac{1}{eR_{\mathrm{N}}}\sum_i\left\{\frac{\partial D_{\mathrm{t}}(\xi_{ij})}{\partial V_j}\left[f(\omega_i)-f(\xi_{ij})\right] - D_{\mathrm{t}}(\xi_{ij})\frac{\partial f(\xi_{ij})}{\partial Vj}\right\}\delta\omega D_{\mathrm{s}}(\omega_i), \tag{4.4}$$

where $\delta\omega$ is the energy spacing and $\xi_{ij} = \omega_i + eV_j$. Note that we dropped the $\Delta_{\mathrm{t}},\gamma_{\mathrm{t}}$ and T dependence for simplicity. The above formula is then solved in a matrix form in order to obtain $D_{\mathrm{s}}(\omega)$.

4.3. Detection of in-gap state in $FeTe_{0.55}Se_{0.45}$

Figure 4.1a shows a topography of the cleaved surface of $FeTe_{0.55}Se_{0.45}$ obtained with a Pb coated tip (see inset). Brighter (darker) regions correspond to Te (Se) terminated areas of the cleaved surface which has a tetragonal crystal structure. Our samples exhibit no excess Fe atoms or clusters on the cleaved surface. Spatially resolved scanning tunneling spectroscopy shows that most locations have a flat gap as shown in Figs. 4.1b-c. However, when we acquire spectra at specific points indicated by black circles ($\mathbf{r}_2$ and $\mathbf{r}_3$) in Fig. 4.1a, we find sharp in-gap states. Figures 4.1d-e and 4.1f-g show such states, both in the raw data as well as in the deconvoluted results. The measured in-gap state is symmetric in energy, i.e. it is visible at $\pm E_{\mathrm{ig}}$ (Fig. 4.1g), or at the Fermi level, $E_{\mathrm{ig}} = 0$ (Fig. 4.1e). In the raw data (before numerical deconvolution) the states are located at energies $\pm(\Delta_{\mathrm{t}} \pm E_{\mathrm{ig}})$ (see arrows in Fig. 4.1d and 4.1f) due to the use of the superconducting tip.

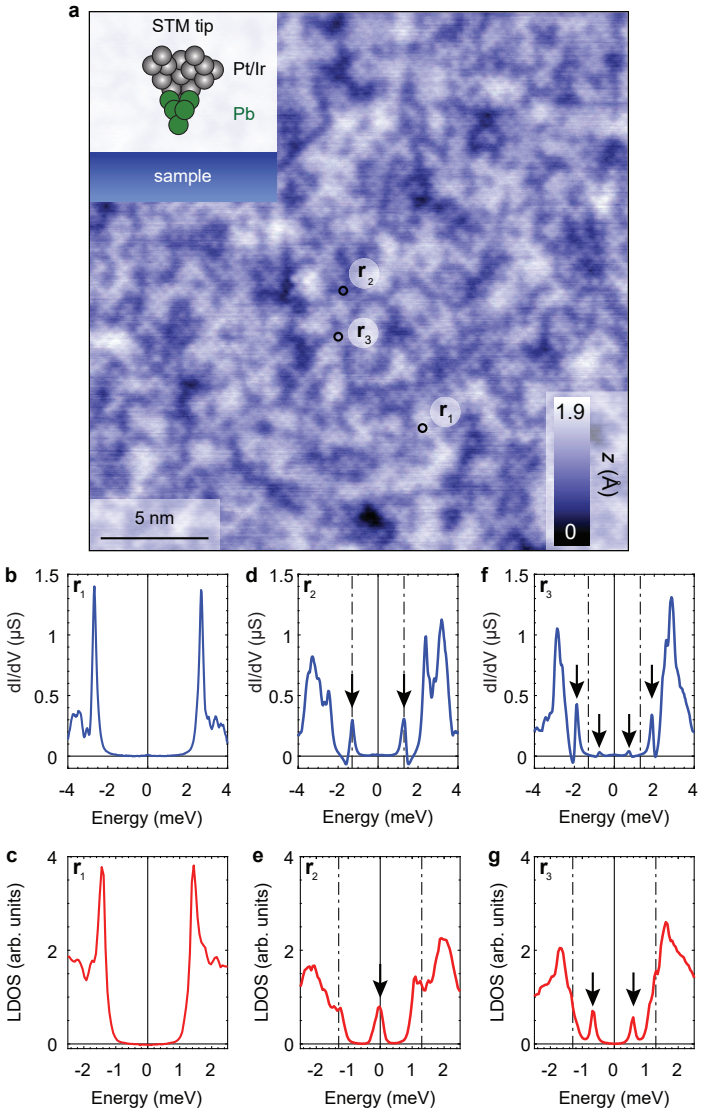

Figure 4.1: **Scanning Tunneling Microscopy on $FeTe_{0.55}Se_{0.45}$ with a superconducting tip. a** Atomically resolved topographic image (z-height map, 25 × 25 nm^2) of $FeTe_{0.55}Se_{0.45}$ cleaved surface acquired with a Pb coated Pt/Ir tip (see inset) at 2.2 K in ultra-high vacuum. Setup condition: $V_{set} = -8$ mV, $I_{set} = -100$ pA. **b, d, f** Average differential conductance spectra in the areas ($\mathbf{r}_1$, $\mathbf{r}_2$, $\mathbf{r}_3$) marked by the black circles in **a**. $\mathbf{r}_1$: no in-gap states. $\mathbf{r}_2$: two in-gap resonances at ± 1.3 meV. $\mathbf{r}_3$: two sets of symmetric peaks around the Fermi level. **c, e, g** Deconvolution of the spectra shown in **b, d, f**, respectively, provide information about the intrinsic LDOS of the sample in the indicated areas. In $\mathbf{r}_2$ a zero-bias impurity state is recovered and in $\mathbf{r}_3$ two in-gap states are observed. Setup conditions: **b** $V_{set} = 6$ mV, $I_{set} = 1.2$ nA, **d, f** $V_{set} = 5$ mV, $I_{set} = 2$ nA. Lock-in modulation is $V_{mod} = 30$ μV peak-to-peak for all measured spectra.

4.4. Spatial dispersion of the in-gap state

In order to characterize the impurity in more detail we acquire a spatially resolved $dI/dV(\mathbf{r}, V)$ map in the area shown in Fig. 4.2a. Three energy layers of the deconvoluted map depicting the LDOS variations are shown in Figs. 4.2b-d. The impurity exhibits a clear ring-shaped feature which eventually becomes a disk with smaller radius at the Fermi level. A spatial line cut profile along the red dashed line shown in Fig. 4.2b reveals two symmetric resonances around zero energy that extend over ~ 10 nm in space (Fig. 4.2e). Importantly, the energies of the in-gap states vary spatially as shown in the spatial cuts (Figs. 4.2e-g) obtained from the same conductance map. The dispersion of the in-gap states shows an X-shaped profile where the crossing point is indicated with $\mathbf{r}_0$ (Fig. 4.2a). In more detail, the state is at zero energy at $\mathbf{r}_0$, and then moves away from the Fermi level, before fading out slightly below the gap edge. We will show later that the character of this dispersion is dependent on the tip-sample distance, and that there can also be zero or two crossing points. By inspecting the topography at $\mathbf{r}_0$ we find no signature of irregularities, which points towards a sub-surface impurity defect as the cause of the observed in-gap peaks in the spectra. We note that these impurities are sparse; we found a total of 5 in a 45×45 nm^2 field-of-view. These all show the same characteristic dispersions, but the X point is estimated at different tip heights. For details, see B.6. Similar observations have been reported previously on $FeTe_{0.55}Se_{0.45}$, but without a clear energy cross at the Fermi level [31, 32].

4.5. YSR impurity states

Our observations are reminiscent of YSR states caused by magnetic impurities in conventional superconductors [35, 38–41]. When a single magnetic impurity is coupled to a superconductor with energy gap Δ via an exchange coupling J then the ground state of the many-body system depends on the interplay between superconductivity and the Kondo effect (described by the Kondo temperature T_K). For $\Delta \gtrsim k_B T_K$ the superconducting ground state prevails (unscreened impurity) whereas for $\Delta < k_B T_K$ the Kondo ground state dominates (screened impurity). In each case, quasiparticle excitations above the ground state give rise to resonances symmetrically around the Fermi level inside the superconducting gap. In an STM experiment, this results in peaks in the conductance spectrum at the energy of the two YSR excitations which is determined by the product $\nu_F JS$, where S is the impurity spin and ν_F the normal state density of states in the superconducting host ($FeTe_{0.55}Se_{0.45}$ in our case).

It is important to note that the $s_\pm$ symmetry of the order parameter in $FeTe_{0.55}Se_{0.45}$ can lead to a very similar phenomenology between magnetic and potential scatterers. While in conventional s-wave superconductors, magnetic impurities are required to create in-gap (YSR) states, in $s_\pm$ superconductors, sub-gap resonances can also occur for non-magnetic scattering centers. This can be shown using different theoretical techniques, including T-matrix method [42, 43], Bogoliubov-de Gennes equations [44, 45] and Green's functions [46–48] applied to multiband systems with $s_\pm$ symmetry.

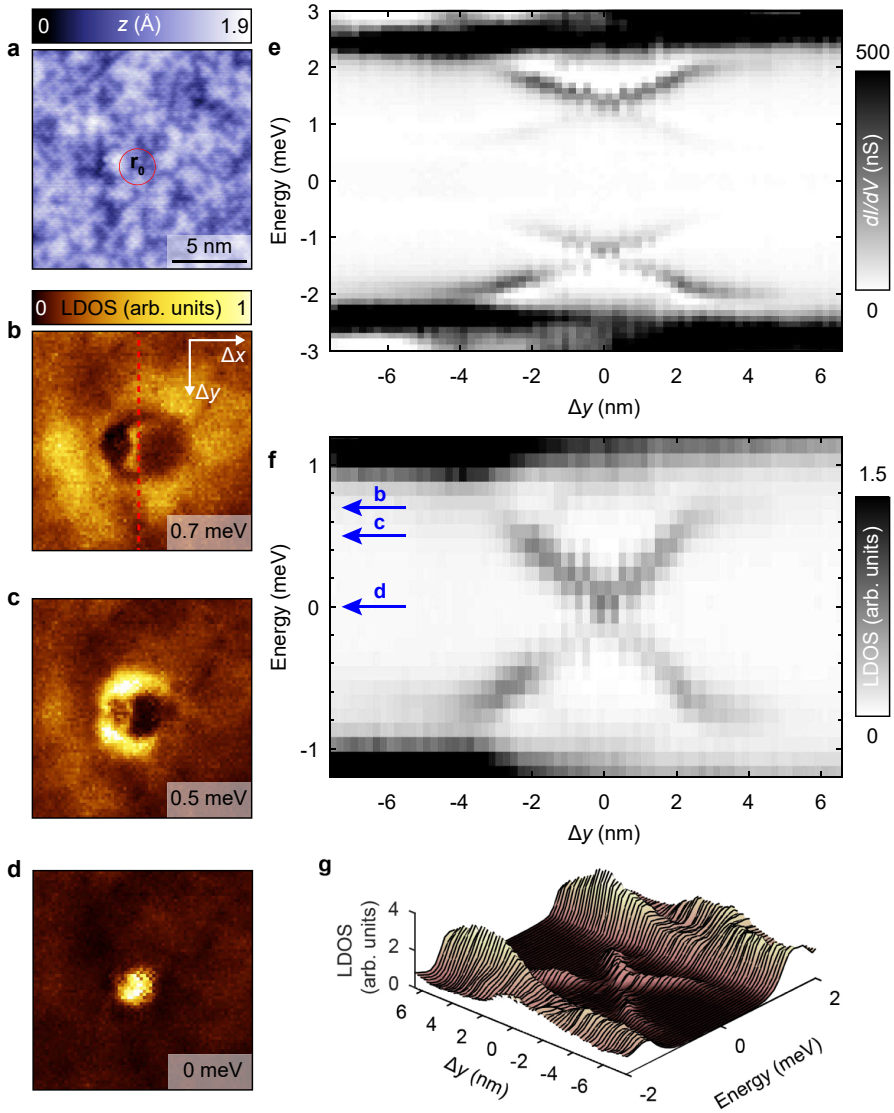

Figure 4.2: **X-shaped spatial dispersion of impurity resonances in** $FeTe_{0.55}Se_{0.45}$**. a** Topographic image at the impurity location ($\mathbf{r}_0$ indicates the impurity center). No clear signature of the impurity is observed. Setup conditions: $V_{\text{set}} = -8$ mV, $I_{\text{set}} = -100$ pA. **b-d** Spatially resolved LDOS maps at different energies obtained by deconvolution of a $dI/dV(\mathbf{r}, V)$ map in the same field-of-view as in **a**. The energy of each LDOS map is indicated at the bottom right corner. **e** Measured differential conductance intensity plot of a vertical linecut passing through the impurity center $\mathbf{r}_0$ ($\Delta y = 0$ nm). The linecut was taken along the red dashed line in **b**. A crossing of the in-gap resonances at the impurity center is observed. Setup conditions: $V_{\text{set}} = -8$ mV, $I_{\text{set}} = -1.6$ nA. Lock-in modulation is $V_{\text{mod}} = 100$ μV peak-to-peak, **f** Deconvolution of the measured spectra in **e** shows an X-shaped dispersion of the sub-gap states crossing the Fermi level at the impurity center. The blue arrows indicate the energy of the maps in **b-d**. **g** Series of LDOS spectra depicting the X-shaped spatial dispersion shown in **f**.

The similarity of magnetic and potential scatterers makes a distinction between these cases more challenging (but possible, with an external magnetic field [30]). In either case, theory predicts energy-symmetric in-gap states with particle-hole asymmetric intensities. The X-shaped phenomenology of the in-gap states shown above shares also similarities with bound-states that have been observed in Pb/Co/Si(111) stacks [49], where they have been interpreted as topological [49, 50]. However, as we will show here, in our experiments the single point of zero bias is just one particular case of a manifold of dispersions that depend on the tip-sample distance.

4.6. Tuning the energy of the in-gap state using the tip

Figure 4.3a shows an intensity plot of a series of spectra above $\mathbf{r}_0$, the location showing the zero-bias impurity state, with changing tip-sample distance (see inset for a schematic). We normalized each spectrum by the normal state resistance $R_{\mathrm{N}} = V_{\mathrm{set}}/I_{\mathrm{set}}$. In order to reduce the distance, we control the tip in constant current feedback and increase the set-point for the current while keeping the voltage bias constant. In addition, we measure the tip-sample distance relative to the set-point: $V_{\mathrm{set}} = 5$ mV, $I_{\mathrm{set}} = 0.4$ nA. Strikingly, we observe a shift in the energy of the in-gap state with varying the tip-sample distance Δd. When the tip is brought closer to the sample surface, the sub-gap resonances shift towards the Fermi energy (Fig. 4.3b) where they cross and split again. We also point out that there is a strong particle-hole asymmetry in the intensity of the in-gap resonances. It can be clearly seen in Fig. 4.3b that the relative intensity between the positive (p) and negative (n) resonances ($I_{\mathrm{p}} - I_{\mathrm{n}}$) changes sign after the cross at the Fermi level. Further, we note that the energy shift for varying Δd is stronger than the spatial dispersion. This can likely be explained by the tip shape, which can be approximated as a sphere of roughly 20 nm. As the tunneling current falls off exponentially with distance, one always tunnels to the point closest to the surface. However, the field is algebraic in the distance, and thus a change horizontally has less of an effect than a change vertically, as shown in B.4.

To obtain a more complete picture of the tuning of the in-gap states as we vary Δd, we measured five $dI/dV(\mathbf{r}, V)$ maps (each at different tip-sample distance) and analyzed azimuthally-averaged radial profiles through the impurity center (Figs. 4.3c-d show two of these profiles. See B.2 for the other 3). We extract the energy of the resonances by Lorentzian fits (Fig. 4.3e), to observe that they cross the Fermi level at the impurity center when being close to the sample. This is the first time that such a crossing has been observed in an unconventional superconductor.

4.7. Microscopic origin

The important question that arises is: what tunes the impurity resonances that we observe? In previous experiments with magnetic ad-atoms or ad-molecules on conventional superconductors [51, 52], it has been shown that the force of the tip changes the coupling between moment and substrate, and that the coupling J and

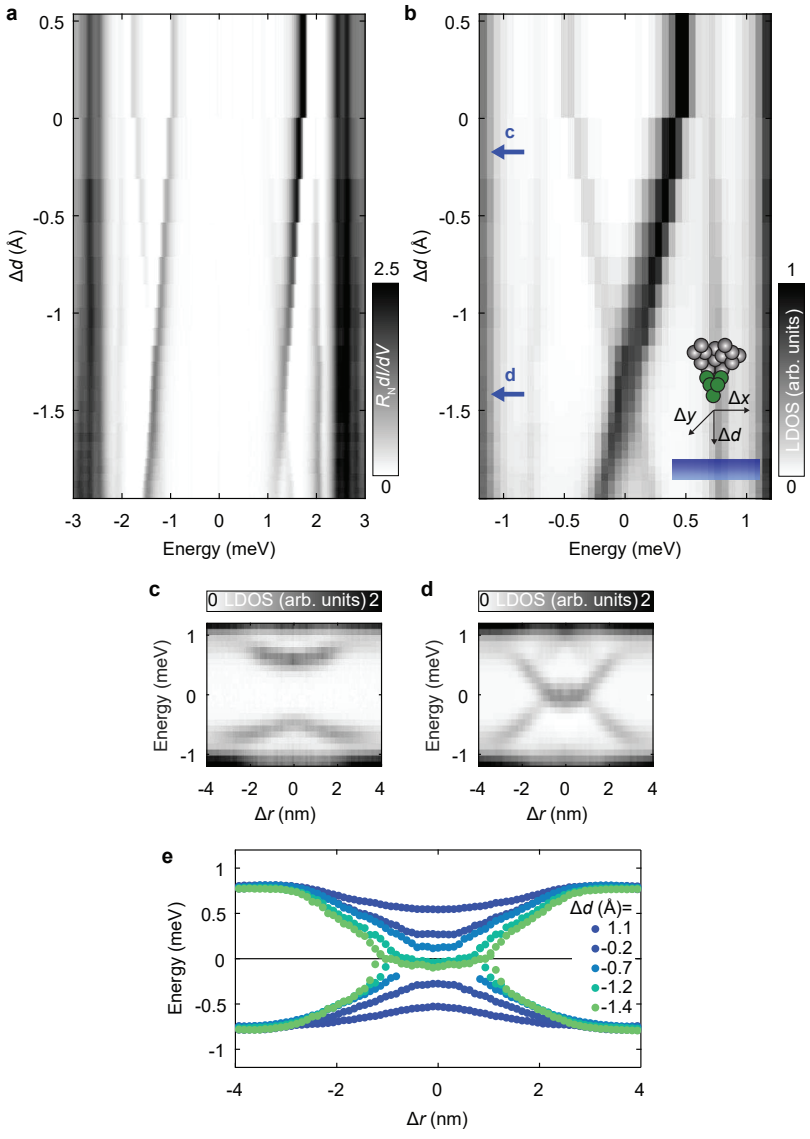

Figure 4.3: **Energy dispersion of the sub-gap resonances as a function of the tip-sample distance. a** Conductance intensity plot for varying tip-sample distance (Δd) normalized by the normal state resistance R_N. The in-gap states disperse and cross at the Fermi level. **b** Same as in **a** for the deconvoluted LDOS data. Inset: schematic representation of the tip movement when we vary the tip-sample distance (Δd) and when the tip scans laterally (Δy and Δx) at a constant height. **c-d** Azimuthally-averaged radial profiles at different tip-sample distances indicated by blue arrows in **b**. Δr, indicates the radial offset $\sqrt{\Delta x^2 + \Delta y^2}$ from the impurity center ($\Delta r = 0$). **e** Energy of the impurity bound state for varying tip-sample distance, extracted by fitting a lorentzian curve in 5 intensity plots (see B.2) similar to **c-d**.

the YSR energy could be tuned in this way. In this case, when the energy crosses the Fermi level at the critical coupling J_C, a first-order quantum phase transition between the singlet (screened) and the doublet (unscreened) ground state is expected [51, 53]. Very recently, a similar force-based scenario has been reported in different systems involving magnetic ad-atoms on top of superconductors [15], including Fe(Te,Se) [30]. As discussed in B.1, a similar scenario can in principle explain the sub-gap dispersion discovered here. However, as the impurity is not loosely bound on top of the surface in the present case, a movement between a sub-surface impurity and the superconductor due to the tip force as the cause for the tuning, seems unlikely. Therefore, we pursue alternative mechanisms. Motivated by the phenomenology of semiconductors [54] or Mott insulators [55], where the tip can act as a local gate electrode (mediated by the poor screening), we propose a similar gating scenario for YSR states in the present case: the electric field of the tip can tune the energy of the impurity state and thus lead to a dispersing YSR state.

First, we note that there can be a significant difference between the work functions of the tip and the sample. Typical work functions are in the range of a few electronvolts, and differences between chemically different materials of the order of an electronvolt are common (see B.4). Hence, it is possible to have a voltage drop between them that is larger than the applied bias. Secondly, the low carrier density in $FeTe_{0.55}Se_{0.45}$ leads to a non-zero screening length giving rise to penetration of the electric field of the tip inside the sample. An estimation of the penetration depth in the sample can be made in the Thomas-Fermi approximation (cf. e.g. [56]). In this framework, the screening length is given by $\lambda_{TF} = (\pi a_0/4k_F)^{1/2}$, where a_0 is the Bohr radius and k_F the Fermi wave-vector. Using reported parameters [11, 12], this yields $\lambda_{TF} = 0.5$ nm, which is comparable to the inter-layer distance [57]. This implies that in principle, an impurity residing between the topmost layers can be affected by the electric field of the tip. In B.4 we further test this possibility by performing an estimate of the potential shift in the impurity, when the tip-sample distance is varied using a simple model for screening (image charges method) to estimate that the shift is comparable to the charging energy of the impurity. We note that this estimate is approximative, as some key parameters are unknown for $FeTe_{0.55}Se_{0.45}$.

Based on these considerations, we conclude that it is possible that the tip acts as a local gate electrode that influences the energy levels of the impurity, which in turn influences the energy of the in-gap states, as we will demonstrate in the modelling carried out below. By adjusting the tip-sample distance the field penetration is modulated leading to an energy shift of the in-gap resonances. The spatial dependence can be explained similarly: when moving the tip over the impurity location, we change the local electric field, which is at a maximum when the tip is right above the impurity. We emphasize that, similar to experiments on semiconductors and Mott insulators, we expect that the details of the gating process depend on the tip shape (see B.4).

4.8. Gate-tunable single-impurity Anderson model

We model the sub-gap state as a YSR state arising from the magnetic moment of a sub-surface impurity level, whose energy is effectively gated by the tip-induced electric field. It should be noted that the sub-gap states arising in an $s_{\pm}$-wave superconductor from a simple non-magnetic impurity can produce a dispersive cross in the in-gap energies as a function of the impurity potential. However, this is only true for a particular range of potentials, and will not generally trace out a single dispersive cross as a function of the impurity strength [44, 46]. Therefore, we are led to conclude that the impurity at hand involves a finite magnetic moment. Local impurity-induced magnetic moments may indeed be particularly prominent in correlated systems like FeSe where even nonmagnetic disorder, in conjunction with electron interactions, can generate local moments [58]. Because of the magnetic nature of the impurity site, the results of our calculations are qualitatively independent on whether we treat the system as an s or $s_{\pm}$-wave superconductor. For simplicity, we perform our calculations assuming standard s-wave pairing.

The superconducting single impurity Anderson model [59] involves an impurity level ϵ_0 with charging energy U coupled via a tunneling rate Γ_s to a superconducting bath with energy gap Δ_s [60–62]. We represent the sample by a simple s-wave Bardeen-Cooper-Schrieffer (BCS) superconductor, and use the zero-bandwidth approximation, including only a single spin-degenerate pair of quasiparticles at energy Δ_s [61, 63]. We further assume that the gating from the tip changes the impurity level ϵ_0 linearly with distance. We then obtain the YSR states by calculating the local impurity spectral function, $D_I(\omega, \epsilon_0)$, as a function of ϵ_0 (and thus of gating) using the Lehmann representation (see B.1 for details).

The result is plotted in Fig. 4.4a, where the observed crossing of the sub-gap states indicates a change between singlet, and a doublet ground state [64]. From the spectral function we can determine the current using leading-order perturbation theory in the tunnel coupling connecting the impurity to the tip, t_t:

$$I(V) = \frac{e|t_t|^2}{\hbar} \int D_t(\omega + eV, \Delta_t, \gamma_t) D_I(\omega, \epsilon_0)[f(\omega, T) - f(\omega + eV, T)]d\omega, \qquad (4.5)$$

here $D_t(\omega, \Delta_t, \gamma_t)$ is the spectral function of the superconducting tip with a finite quasiparticle broadening incorporated as a Dynes parameter [65], γ_t and $\hbar$ the reduced Planck's constant. A phenomenological relaxation rate, Γ_r, is incorporated into the Lehmann representation, (see B.1), to construct $D_I(\omega, \epsilon_0)$. This parameter accounts for quasiparticle relaxation of the YSR resonances at $\omega = \pm E_{ig}$. The validity of the expansion in $\Gamma_t = \pi \nu_F |t_t|^2$, which captures only single electron transport and omits Andreev reflections, rests on the assumption that the sub-gap state thermalizes with rate Γ_r between each tunneling event. In the opposite limit, $\Gamma_t \gg \Gamma_r$, transport takes place via resonant Andreev reflections, and the sub-gap conductance peaks at $eV = \pm(\Delta_t + E_{ig})$ display a bias asymmetry that is reversed compared to the bias asymmetry of the single electron transport regime [41]. In principle, these two regimes can be differentiated by varying Γ_t, since the conductance peaks increase linearly with Γ_t in the single electron regime, and sublinearly in the resonant Andreev regime [41, 66]. The experimental data shown in Fig. 4.3 display a

marked asymmetry, consistent with our assumption of relaxation dominated transport where conductance asymmetry will follow the asymmetry of the underlying spectral function.

Next, we investigate the situations where the tip moves over the impurity along the surface, or towards the impurity as a function of tip-sample distance Δd. These situations are marked with blue and red arrows in Fig. 4.4a, respectively. In Figs. 4.4b-c we then plot sub-gap conductance as a function of level position, ϵ_0, corresponding to the red/blue traces, assuming a linear dependence of ϵ_0 with tip-sample distance. The agreement between our model and the data is good, both in terms of the energy dispersion and the asymmetry. Also, in both experiment and theory, additional conductance peaks at $eV = \pm(\Delta_t - E_{ig})$ are visible close to the singlet-doublet phase transition. We interpret these lines as the additional single electron processes shown in Fig. 4.4d, which arise from thermal population of the excited state close to the phase transition where $E_{ig} \lesssim k_B T$. The conductance peaks at $\Delta_t \pm E_{ig}$ meet at the point where the YSR states cross zero energy, signaling the change between singlet, and doublet ground states, and the asymmetry in intensity between the conductance peaks at $eV = \pm(\Delta_t + E_{ig})$ switches around.

The good agreement between this simple model (Figs. 4.4b-c) and the data presented in Figs. 4.2e and 4.3a, supports our interpretation that the tip exerts an effective gating of the impurity. We discuss alternative scenarios further in B.1, but the fact that our impurity is below the surface and the excellent agreement between the model and the data lead us to conclude that the gating scenario is most likely in the present case.

4.9. Conclusions and outlook

In summary, we have reported on the properties of energy symmetric in-gap states in $FeTe_{0.55}Se_{0.45}$ that can be tuned through the Fermi level. These states extend over a large (~ 10 nm) area around the center locations. Our data point towards a sub-surface magnetic impurity embedded in a low-density superfluid with large screening length that leads to YSR-like in-gap states. We propose a novel tip-gating mechanism for the dispersion and perform calculations within the single impurity Anderson model that show excellent agreement with the data. Such a mechanism could also play a role in previous experiments on elemental superconductors or heterostructures. How such states are related to the topological superconductivity in $FeTe_{0.55}Se_{0.45}$ remains an open question. Our work further shows that one needs to be careful when interpreting zero-bias peaks in putative topological states, and junction resistance dependent experiments are a necessary – ideally combinded with other techniques such as noise spectroscopy [67–69] (see also B.3), spin-polarized STM [70], or photon-assisted tunneling [71] will allow for better understanding. Independent of this, tunable impurity states like the one we report here could offer a platform to study quantum phase transitions, impurity scattering, and the screening behavior of superfluids.

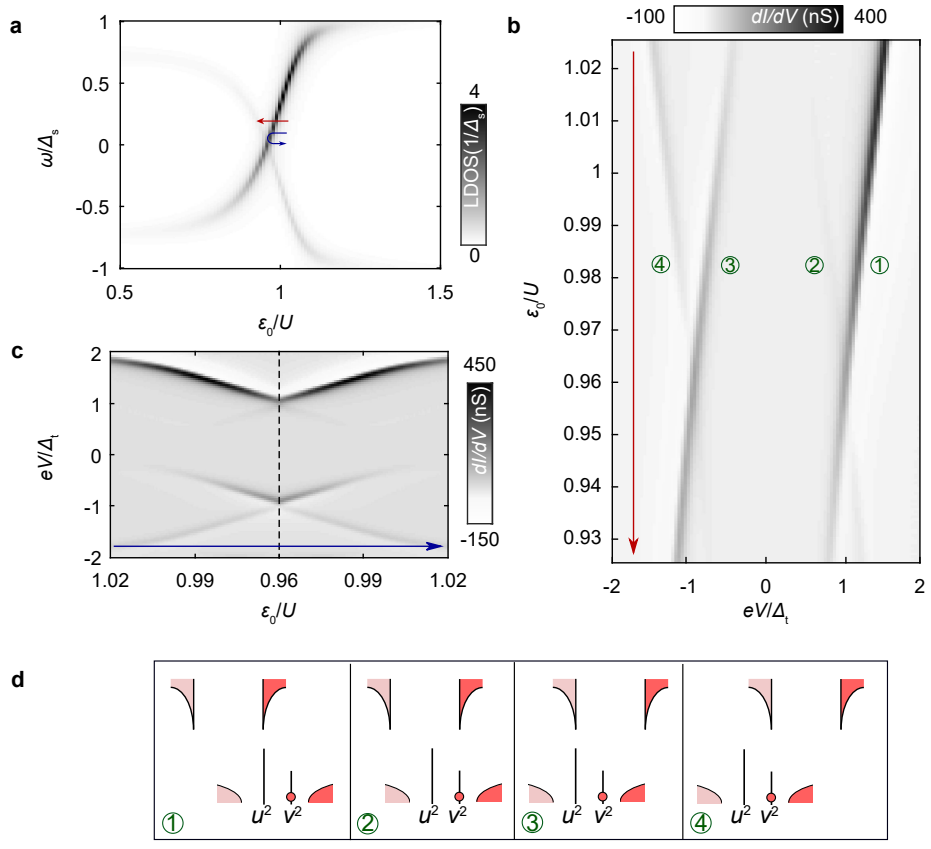

Figure 4.4: **Anderson impurity model for Yu-Shiba-Rusinov bound states.** **a** Local density of states as a function of level energy ϵ_0. The impurity spectral function was calculated within the zero-bandwidth approximation using the Lehmann spectral representation for the retarded Green's function (see B.1). Red and blue lines indicate the two different ϵ_0 sweeps plotted in **b** and **c**, respectively. **b-c** Relaxation dominated tunneling conductance calculated to leading order in the tip-impurity tunneling rate Γ_t. Labels in **b** refer to processes in **d**. The dashed line in **c** shows the turning point of the blue line in **a**. **d** Guide to the eye for different conductance contributions in **b** and **c**. Processes 2-3 require a finite population of the excited state, in this case supplied by temperature. For all panels we use $U = 20$, $\Gamma_s = 3$, $\Gamma_t = 0.04$, $\gamma = \Gamma_r = 0.035$ and $k_B T = 0.2$, all in units of Δ_s.

References

[1] M. Bendele, S. Weyeneth, R. Puzniak, A. Maisuradze, E. Pomjakushina, K. Conder, V. Pomjakushin, H. Luetkens, S. Katrych, A. Wisniewski, R. Khasanov, and H. Keller, *Anisotropic superconducting properties of single-crystalline* $\mathrm{FeSe_{0.5}Te_{0.5}}$, Phys. Rev. B **81**, 224520 (2010).

[2] C. C. Homes, Y. M. Dai, J. S. Wen, Z. J. Xu, and G. D. Gu, $\mathrm{FeTe_{0.55}Se_{0.45}}$*: A multiband superconductor in the clean and dirty limit,* Phys. Rev. B **91**, 144503 (2015).

[3] D. Cho, K. Bastiaans, D. Chatzopoulos, G. D. Gu, and M. P. Allan, *A strongly inhomogeneous superfluid in an iron-based superconductor,* Nature **571**, 541 (2019).

[4] Y. Lubashevsky, E. Lahoud, K. Chashka, D. Podolsky, and A. Kanigel, *Shallow pockets and very strong coupling superconductivity in* $\mathrm{FeSe}_x\mathrm{Te}_{1-x}$, Nat. Phys. **8**, 309 (2012).

[5] S. Rinott, K. B. Chashka, A. Ribak, E. D. L. Rienks, A. Taleb-Ibrahimi, P. Le Fevre, F. Bertran, M. Randeria, and A. Kanigel, *Tuning across the BCS-BEC crossover in the multiband superconductor* $\mathrm{Fe}_{1+y}\mathrm{Se}_x\mathrm{Te}_{1-x}$*: An angle-resolved photoemission study,* Sci. Adv. **3** (2017).

[6] H. Miao, W. H. Brito, Z. P. Yin, R. D. Zhong, G. D. Gu, P. D. Johnson, M. P. M. Dean, S. Choi, G. Kotliar, W. Ku, X. C. Wang, C. Q. Jin, S.-F. Wu, T. Qian, and H. Ding, *Universal* $2\Delta_{\max}/k_{\mathrm{B}}T_{\mathrm{c}}$ *scaling decoupled from the electronic coherence in iron-based superconductors,* Phys. Rev. B **98**, 020502 (2018).

[7] A. Kreisel, P. J. Hirschfeld, and B. M. Andersen, *On the remarkable superconductivity of FeSe and its close cousins,* Symmetry **12**, 1 (2020).

[8] X. Wu, S. Qin, Y. Liang, H. Fan, and J. Hu, *Topological characters in* $\mathrm{Fe(Te}_{1-x}\mathrm{Se}_x)$ *thin films,* Phys. Rev. B **93**, 115129 (2016).

[9] Z. Wang, P. Zhang, G. Xu, L. K. Zeng, H. Miao, X. Xu, T. Qian, H. Weng, P. Richard, A. V. Fedorov, H. Ding, X. Dai, and Z. Fang, *Topological nature of the* $\mathrm{FeSe_{0.5}Te_{0.5}}$ *superconductor,* Phys. Rev. B **92**, 115119 (2015).

[10] G. Xu, B. Lian, P. Tang, X.-L. Qi, and S.-C. Zhang, *Topological Superconductivity on the Surface of Fe-Based Superconductors,* Phys. Rev. Lett. **117**, 047001 (2016).

[11] P. Zhang, K. Yaji, T. Hashimoto, Y. Ota, T. Kondo, K. Okazaki, Z. Wang, J. Wen, G. D. Gu, H. Ding, and S. Shin, *Observation of topological superconductivity on the surface of an iron-based superconductor,* Science **360**, 182 (2018).

[12] D. Wang, L. Kong, P. Fan, H. Chen, S. Zhu, W. Liu, L. Cao, Y. Sun, S. Du, J. Schneeloch, R. Zhong, G. Gu, L. Fu, H. Ding, and H.-J. Gao, *Evidence for Majorana bound states in an iron-based superconductor,* Science **362**, 333 (2018).

[13] S. Zhu, L. Kong, L. Cao, H. Chen, M. Papaj, S. Du, Y. Xing, W. Liu, D. Wang, C. Shen, F. Yang, J. Schneeloch, R. Zhong, G. Gu, L. Fu, Y.-Y. Zhang, H. Ding, and H.-J. Gao, *Nearly quantized conductance plateau of vortex zero mode in an iron-based superconductor,* Science **367**, 189 (2020).

[14] M. Chen, X. Chen, H. Yang, Z. Du, X. Zhu, E. Wang, and H. H. Wen, *Discrete energy levels of Caroli-de Gennes-Matricon states in quantum limit in* $FeTe_{0.55}Se_{0.45}$, Nat. Commun. **9**, 970 (2018).

[15] H. Huang, R. Drost, J. Senkpiel, C. Padurariu, B. Kubala, A. L. Yeyati, J. C. Cuevas, J. Ankerhold, K. Kern, and C. R. Ast, *Quantum phase transitions and the role of impurity-substrate hybridization in Yu-Shiba-Rusinov states,* Commun. Phys. **3**, 199 (2020).

[16] G. C. Ménard, S. Guissart, C. Brun, S. Pons, V. S. Stolyarov, F. Debontridder, M. V. Leclerc, E. Janod, L. Cario, D. Roditchev, P. Simon, and T. Cren, *Coherent long-range magnetic bound states in a superconductor,* Nat. Phys. **11**, 1013 (2015).

[17] B. W. Heinrich, J. I. Pascual, and K. J. Franke, *Single magnetic adsorbates on s-wave superconductors,* Prog. Surf. Sci. **93**, 1 (2018).

[18] E. W. Hudson, K. M. Lang, V. Madhavan, S. H. Pan, H. Eisaki, S. Uchida, and J. C. Davis, *Interplay of magnetism and high-T_c superconductivity at individual Ni impurity atoms in* $Bi_2Sr_2CaCu_2O_{8+\delta}$, Nature **411**, 920 (2001).

[19] B. B. Zhou, S. Misra, E. H. da Silva Neto, P. Aynajian, R. E. Baumbach, J. D. Thompson, E. D. Bauer, and A. Yazdani, *Visualizing nodal heavy fermion superconductivity in* $CeCoIn_5$, Nat. Phys. **9**, 474 (2013).

[20] J. E. Hoffman, K. McElroy, D. H. Lee, K. M. Lang, H. Eisaki, S. Uchida, and J. C. Davis, *Imaging quasiparticle interference in* $Bi_2Sr_2CaCu_2O_{8+\delta}$, Science **297**, 1148 (2002).

[21] M. P. Allan, F. Massee, D. K. Morr, J. V. Dyke, A. W. Rost, A. P. Mackenzie, C. Petrovic, and J. C. Davis, *Imaging Cooper pairing of heavy fermions in* $CeCoIn_5$, Nat. Phys. **9**, 468 (2013).

[22] M. P. Allan, T.-M. Chuang, F. Massee, Y. Xie, N. Ni, S. Bud'Ko, G. Boebinger, Q. Wang, D. Dessau, P. Canfield, M. Golden, and J. Davis, *Anisotropic impurity states, quasiparticle scattering and nematic transport in underdoped* $Ca(Fe_{1-x}Co_x)_2As_2$, Nat. Phys. **9**, 220 (2013).

[23] E. P. Rosenthal, E. F. Andrade, C. J. Arguello, R. M. Fernandes, L. Y. Xing, X. C. Wang, C. Q. Jin, A. J. Millis, and A. N. Pasupathy, *Visualization of electron nematicity and unidirectional antiferroic fluctuations at high temperatures in NaFeAs,* Nat. Phys. **10**, 225 (2014).

[24] H. Beidenkopf, P. Roushan, J. Seo, L. Gorman, I. Drozdov, Y. S. Hor, R. J. Cava, and A. Yazdani, *Spatial fluctuations of helical Dirac fermions on the surface of topological insulators,* Nat. Phys. **7**, 939 (2011).

[25] D. Sticlet and C. Morari, *Topological superconductivity from magnetic impurities on monolayer* $NbSe_2$*,* Phys. Rev. B **100**, 075420 (2019).

[26] A. Palacio-Morales, E. Mascot, S. Cocklin, H. Kim, S. Rachel, D. K. Morr, and R. Wiesendanger, *Atomic-scale interface engineering of Majorana edge modes in a 2D magnet-superconductor hybrid system,* Sci. Adv. **5** (2019).

[27] K. Pöyhönen, I. Sahlberg, A. Weststrom, and T. Ojanen, *Amorphous topological superconductivity in a Shiba glass,* Nat. Commun. **9**, 2103 (2018).

[28] S. Nadj-Perge, I. K. Drozdov, J. Li, H. Chen, S. Jeon, J. Seo, A. H. MacDonald, B. A. Bernevig, and A. Yazdani, *Observation of Majorana fermions in ferromagnetic atomic chains on a superconductor,* Science **346**, 602 (2014).

[29] J.-X. Yin, Z. Wu, J.-H. Wang, Z.-Y. Ye, J. Gong, X.-Y. Hou, L. Shan, A. Li, X.-J. Liang, X.-X. Wu, J. Li, C.-S. Ting, Z.-Q. Wang, J.-P. Hu, P.-H. Hor, H. Ding, and S. H. Pan, *Observation of a robust zero-energy bound state in iron-based superconductor Fe(Te,Se),* Nat. Phys. **11**, 543 (2015).

[30] P. Fan, F. Yang, G. Qian, H. Chen, Y. Y. Zhang, G. Li, Z. Huang, Y. Xing, L. Kong, W. Liu, K. Jiang, C. Shen, S. Du, J. Schneeloch, R. Zhong, G. Gu, Z. Wang, H. Ding, and H. J. Gao, *Observation of magnetic adatom-induced Majorana vortex and its hybridization with field-induced Majorana vortex in an iron-based superconductor,* Nat. Commun. **12**, 1348 (2021).

[31] T. Machida, Y. Sun, S. Pyon, S. Takeda, Y. Kohsaka, T. Hanaguri, T. Sasagawa, and T. Tamegai, *Zero-energy vortex bound state in the superconducting topological surface state of Fe(Se,Te),* Nat. Mater. **18**, 811 (2019).

[32] Z. Wang, J. O. Rodriguez, L. Jiao, S. Howard, M. Graham, G. D. Gu, T. L. Hughes, D. K. Morr, and V. Madhavan, *Evidence for dispersing 1D Majorana channels in an iron-based superconductor,* Science **367**, 104 (2020).

[33] S. H. Pan, E. W. Hudson, and J. C. Davis, *Vacuum tunneling of superconducting quasiparticles from atomically sharp scanning tunneling microscope tips,* Appl. Phys. Lett. **73**, 2992 (1998).

[34] J. G. Rodrigo, H. Suderow, and S. Vieira, *On the use of STM superconducting tips at very low temperatures,* Eur. Phys. J. B **40**, 483 (2004).

[35] K. J. Franke, G. Schulze, and J. I. Pascual, *Competition of Superconducting Phenomena and Kondo Screening at the Nanoscale,* Science **332**, 940 (2011).

[36] D.-J. Choi, C. Rubio-Verdú, J. de Bruijckere, M. M. Ugeda, N. Lorente, and J. I. Pascual, *Mapping the orbital structure of impurity bound states in a superconductor,* Nat. Commun. **8**, 15175 (2017).

[37] J.-D. Pillet, C. H. L. Quay, P. Morfin, C. Bena, A. L. Yeyati, and P. Joyez, *Andreev bound states in supercurrent-carrying carbon nanotubes revealed,* Nat. Phys. **6**, 965 (2010).

[38] L. Yu, *Bound state in superconductors with paramagnetic impurities,* Acta. Phys. Sin. **21**, 75 (1965).

[39] H. Shiba, *Classical Spins in Superconductors,* Prog. Theor. Phys. **40**, 435 (1968).

[40] A. Rusinov, *Superconcductivity near a Paramagnetic Impurity,* J. Exp. Theor. Phys. **9**, 85 (1969).

[41] M. Ruby, F. Pientka, Y. Peng, F. von Oppen, B. W. Heinrich, and K. J. Franke, *Tunneling Processes into Localized Subgap States in Superconductors,* Phys. Rev. Lett. **115**, 087001 (2015).

[42] Y. Bang, H.-Y. Choi, and H. Won, *Impurity effects on the $\pm s$-wave state of the iron-based superconductors,* Phys. Rev. B **79**, 054529 (2009).

[43] A. Kreisel, R. Nelson, T. Berlijn, W. Ku, R. Aluru, S. Chi, H. Zhou, U. R. Singh, P. Wahl, R. Liang, W. N. Hardy, D. A. Bonn, P. J. Hirschfeld, and B. M. Andersen, *Towards a quantitative description of tunneling conductance of superconductors: Application to LiFeAs,* Phys. Rev. B **94**, 224518 (2016).

[44] T. Kariyado and M. Ogata, *Single-Impurity Problem in Iron-Pnictide Superconductors,* J. Phys. Soc. Japan **79**, 16 (2010).

[45] W.-F. Tsai, Y.-Y. Zhang, C. Fang, and J. Hu, *Impurity-induced bound states in iron-based superconductors with s-wave cos $k_x \cdot$ cos k_y pairing symmetry,* Phys. Rev. B **80**, 064513 (2009).

[46] M. N. Gastiasoro, P. J. Hirschfeld, and B. M. Andersen, *Impurity states and cooperative magnetic order in Fe-based superconductors,* Phys. Rev. B **88**, 220509 (2013).

[47] T. K. Ng and Y. Avishai, *In-gap bound states induced by nonmagnetic impurities in two-band $s_\pm$ superconductors,* Phys. Rev. B **80**, 104504 (2009).

[48] R. Beaird, I. Vekhter, and J.-X. Zhu, *Impurity states in multiband s-wave superconductors: Analysis of iron pnictides,* Phys. Rev. B **86**, 140507 (2012).

[49] G. C. Ménard, S. Guissart, C. Brun, R. T. Leriche, M. Trif, F. Debontridder, D. Demaille, D. Roditchev, P. Simon, and T. Cren, *Two-dimensional topological superconductivity in Pb/Co/Si(111),* Nat. Commun. **8**, 2040 (2017).

[50] M. Garnier, A. Mesaros, and P. Simon, *Topological superconductivity with deformable magnetic skyrmions,* Commun. Phys. **2**, 126 (2019).

[51] L. Farinacci, G. Ahmadi, G. Reecht, M. Ruby, N. Bogdanoff, O. Peters, B. W. Heinrich, F. von Oppen, and K. J. Franke, *Tuning the Coupling of an Individual Magnetic Impurity to a Superconductor: Quantum Phase Transition and Transport,* Phys. Rev. Lett. **121**, 196803 (2018).

[52] L. Malavolti, M. Briganti, M. Hänze, G. Serrano, I. Cimatti, G. McMurtrie, E. Otero, P. Ohresser, F. Totti, M. Mannini, R. Sessoli, and S. Loth, *Tunable Spin–Superconductor Coupling of Spin 1/2 Vanadyl Phthalocyanine Molecules,* Nano Lett. **18**, 7955 (2018).

[53] A. V. Balatsky, I. Vekhter, and J.-X. Zhu, *Impurity-induced states in conventional and unconventional superconductors,* Rev. Mod. Phys. **78**, 373 (2006).

[54] A. P. Wijnheijmer, J. K. Garleff, K. Teichmann, M. Wenderoth, S. Loth, and P. M. Koenraad, *Single Si dopants in GaAs studied by scanning tunneling microscopy and spectroscopy,* Phys. Rev. B **84**, 125310 (2011).

[55] I. Battisti, V. Fedoseev, K. M. Bastiaans, A. de la Torre, R. S. Perry, F. Baumberger, and M. P. Allan, *Poor electronic screening in lightly doped Mott insulators observed with scanning tunneling microscopy,* Phys. Rev. B **95**, 235141 (2017).

[56] T. Koyama, *Comment on "Charge expulsion and electric field in superconductors",* Phys. Rev. B **70**, 226503 (2004).

[57] B. C. Sales, A. S. Sefat, M. A. McGuire, R. Y. Jin, D. Mandrus, and Y. Mozharivskyj, *Bulk superconductivity at 14 K in single crystals of* $Fe_{1+y}Te_xSe_{1-x}$, Phys. Rev. B **79**, 094521 (2009).

[58] S. Y. Song, J. H. J. Martiny, A. Kreisel, B. M. Andersen, and J. Seo, *Visualization of Local Magnetic Moments Emerging from Impurities in Hund's Metal States of FeSe,* Phys. Rev. Lett. **124**, 117001 (2020).

[59] P. W. Anderson, *Theory of localized magnetic states in metals,* J. Appl. Phys. **37**, 1194 (1966).

[60] A. Jellinggaard, K. Grove-Rasmussen, M. H. Madsen, and J. Nygård, *Tuning Yu-Shiba-Rusinov states in a quantum dot,* Phys. Rev. B **94**, 064520 (2016).

[61] G. Kiršanskas, M. Goldstein, K. Flensberg, L. I. Glazman, and J. Paaske, *Yu-Shiba-Rusinov states in phase-biased superconductor–quantum dot–superconductor junctions,* Phys. Rev. B **92**, 235422 (2015).

[62] R. Žitko, *Numerical subgap spectroscopy of double quantum dots coupled to superconductors,* Phys. Rev. B **91**, 165116 (2015).

[63] K. Grove-Rasmussen, G. Steffensen, A. Jellinggaard, M. H. Madsen, R. Žitko, J. Paaske, and J. Nygård, *Yu-Shiba-Rusinov screening of spins in double quantum dots,* Nat. Commun. **9**, 2376 (2018).

[64] J. Bauer, A. Oguri, and A. C. Hewson, *Spectral properties of locally correlated electrons in a Bardeen–Cooper–Schrieffer superconductor,* J. Phys. Condens. Matter **19**, 486211 (2007).

[65] R. C. Dynes, V. Narayanamurti, and J. P. Garno, *Direct Measurement of Quasiparticle-Lifetime Broadening in a Strong-Coupled Superconductor,* Phys. Rev. Lett. **41**, 1509 (1978).

[66] H. Huang, C. Padurariu, J. Senkpiel, R. Drost, A. L. Yeyati, J. C. Cuevas, B. Kubala, J. Ankerhold, K. Kern, and C. R. Ast, *Tunneling dynamics between superconducting bound states at the atomic limit,* Nat. Phys. (2020).

[67] T. Jonckheere, J. Rech, A. Zazunov, R. Egger, A. L. Yeyati, and T. Martin, *Giant Shot Noise from Majorana Zero Modes in Topological Trijunctions,* Phys. Rev. Lett. **122**, 97003 (2019).

[68] A. Golub and B. Horovitz, *Shot noise in a Majorana fermion chain,* Phys. Rev. B **83**, 153415 (2011).

[69] K. M. Bastiaans, D. Cho, D. Chatzopoulos, M. Leeuwenhoek, C. Koks, and M. P. Allan, *Imaging doubled shot noise in a Josephson scanning tunneling microscope,* Phys. Rev. B **100**, 104506 (2019).

[70] R. Wiesendanger, *Spin mapping at the nanoscale and atomic scale,* Rev. Mod. Phys. **81**, 1495 (2009).

[71] H.-Z. Tang, Y.-T. Zhang, and J.-J. Liu, *Photon-assisted tunneling through a topological superconductor with Majorana bound states,* AIP Advances **5**, 127129 (2015).